Scripta Materialia 120 (2016) 37–40

Contents lists available at ScienceDirect

Scripta Materialia

journal homepage: www.elsevier.com/locate/scriptamat

Regular Article

Plasticity of lath martensite by sliding of substructure boundaries

C. Du, J.P.M. Hoefnagels *, R. Vaes, M.G.D. Geers

Department of Mechanical Engineering, Eindhoven University of Technology, P.O. Box 513, 5600 MB Eindhoven, The Netherlands

ARTICLE INFO

Article history:
Received 29 January 2016
Received in revised form 4 April 2016
Accepted 4 April 2016
Available online 22 April 2016

Keywords:
Lath martensite
Micro-tensile testing
Plasticity
Boundary sliding

ABSTRACT

Well-defined uniaxial micro-tensile tests were performed on lath martensite with different types of substructure boundaries (block, sub-block and lath boundaries) tilted with respect to the loading direction. A characteristic deformation mechanism of lath martensite is hereby identified, i.e. sliding along the substructure boundaries. This boundary sliding can occur at all types of boundaries at relatively low stresses. Internal boundaries not only strengthen lath martensite, as well established in literature, but under favorable orientations also mitigate plastic deformation. The overall plastic deformation results from the competition of crystallographic slip with boundary sliding.

Lath martensite, the most typical morphology of martensite, is the prime constituent that elevates the strength in high strength steels. It has high industrial relevance as it is present in e.g. dual-phase (DP) steel, transformation-induced plasticity steel, and quenching-partitioning steel. Lath martensite has a complex hierarchical microstructure in which a prior austenite grain is divided into packets, packets subdivided into blocks, and blocks into sub-blocks each containing multiple laths [1]. This leads to many internal boundaries, which influence the mechanical properties of lath martensite strongly [2].

Lath martensite mechanics has been studied to limited extent, in part due to the complexity of small-scale experimentation. From macroscopic tensile tests, Morito et al. and Zhang et al. found that a Hall-Petch relation holds between the yield strength and block size [3,4]. From nano- and micro-indentation tests, Ohmura et al. concluded that the block structure increases the hardness [5,6]. From micro-bending tests, Shibata et al. [7,8] reported that block boundaries are the most effective barriers to dislocation motion, which was also concluded by Ghassemi-Armaki et al. and Mine et al. from, respectively, micro-compression and micro-tension tests [9–11]. Recently our micro-tensile tests on well-defined multi-block and single-block specimens showed that sub-block boundary strengthening is almost equally important as block boundary strengthening [12].

In general, research mentioned above focused on the strengthening effects of lath martensite boundaries caused by their interaction with dislocations during plastic deformation. Yet, plasticity was also found to occur parallel to the (tilted) lath boundaries, although at large strains crystallographic slip cuts across the boundaries [13,14]. The former may be related to the Kurdjumov-Sachs transformation orientation relationship through which two BCC slip systems in each martensite lath are closely aligned to the neighboring boundary. Additionally, in lath-martensite-containing engineering steels, the small martensite islands typically do not contain all variants, while a single (tilted) boundary often reaches across the small martensite ligaments, which is highly relevant for the overall mechanics [15,16]. In such a configuration, crystallographic slip does not cross the boundary to accommodate ligament stretching, especially because two slip systems are aligned with each boundary. Consequently, the role of internal boundaries may differ substantially from the strengthening mechanism suggested in literature.

This work studies the micro-mechanical role of substructure boundaries in lath martensite, in configurations where crystallographic slip is not forced to cut across the boundaries. Therefore, *in-situ* uniaxial micro-tensile tests are performed on single-packet specimens containing different types of boundaries that are all tilted at approximately 45° to the loading direction, there by simulating the loading of tilted boundary regions in fully martensitic steel and small ligaments in martensite islands. Interestingly, a new deformation micro-mechanism other than crystallographic slip will be revealed.

The lath martensite specimens (0.092C-1.68Mn-0.24Si-0.57Cr) were produced by 2-hour heating at 1000 °C, followed by water quenching, yielding large packets well suited for fabrication of single-packet specimens. The test procedure involves [17]: (i) wedge fabrication from lath martensite sheet by grinding/polishing/electrochemical etching, (ii) careful selection of specimen locations at the wedge tip using large-area EBSD, (iii) accurate focused-ion-beam (FIB) milling of micro-tensile specimens with constant (3.0×2.5 μm) cross-section (Fig. 1d), (iv) detailed top- and bottom-side EBSD analysis of each specimen, enabling Schmid factor analysis (Table 1), (v) uniaxial tensile tests with highly accuracy in specimen alignment (<0.1 mrad

* Corresponding author.
E-mail address: j.p.m.hoefnagels@tue.nl (J.P.M. Hoefnagels).

http://dx.doi.org/10.1016/j.scriptamat.2016.04.006
1359-6462/

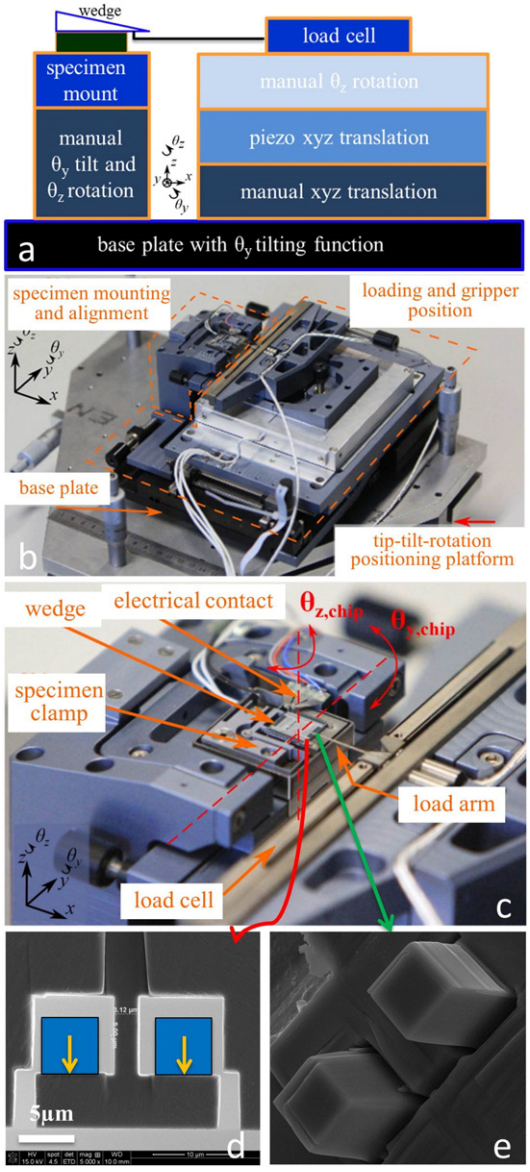

Fig. 1. (a, b) A schematic drawing and real image of the nano-force tensile stage [12,18], with the specimen on the left and loading block on the right, (c) zoom of the load cell and specimen holder, (d) top view of the micro-tensile specimen at the wedge tip, with the two-teeth gripper drawn in blue, and (e) detailed zoom of the two-teeth gripper at the end of the load arm.

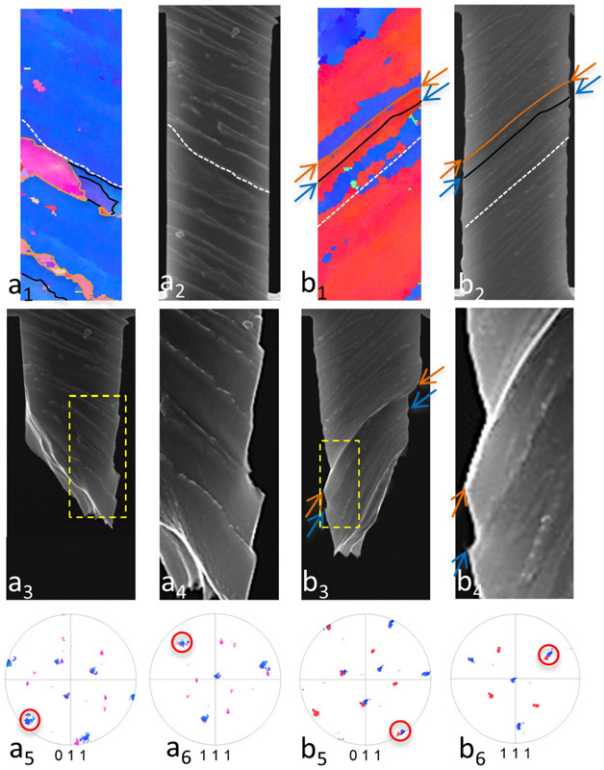

Fig. 2. Two 9 μm-long specimens with tilted boundaries to the loading direction shown with inverse pole figure orientation map (a_1, b_1), SEM pictures before loading (a_2, b_2) and after facture (a_3, b_3) together with a zoom (yellow frame) of the fractured specimens (a_4, b_4). The red circles in the {110} (a_5, b_5) and {111} (a_6, b_6) pole figures indicate the favored slip system. Block and sub-block boundaries are marked with orange and black lines respectively; the fracture surface with a white dotted line. The many lath boundaries are not marked. The arrows in b_1–b_4 indicate sliding boundaries.

angular alignment and near-perfect co-linearity) and force (from 0.07 μN to 250 mN) and displacement (<6 nm reproducibility) measurement (Fig. 1a–c) [18], under (vi) *in-situ* optical microscopy enabling microscopic slip trace analysis.

In all EBSD maps, the type of boundaries (block or sub-block) was analyzed from the boundary misorientation (respectively $\Delta\theta > 12°$, $5 < \Delta\theta < 12°$) and is consistently marked with different line colors: *orange* and *black* for, respectively, block and sub-block boundaries. Laths within one sub-block have almost identical orientation, making their boundaries invisible in EBSD maps. For the first sample batch, the top and bottom sides were milled flat to yield the best EBSD quality, at the expense of invisible topographic contrast of the lath boundaries due to etching-induced surface traces. Therefore, a second batch of specimens was fabricated without topside milling, for which the lath boundaries are identified. It was confirmed that (almost all) lath-, sub-block-, and block-boundaries in one packet are (approximately) parallel.

Starting with the second batch, Fig. 2 shows the topsides of two samples both before and after plastic deformation and the {110} and {111} inverse pole figures of the undeformed state. Fig. 2a_{1-6} shows a single-packet sample, of predominantly one block, with block boundaries and sub-block boundaries that are (i) tilted to the loading direction, (ii) aligned with one (110) martensite plane corresponding to a (111) prior-austenite plane, and (iii) roughly perpendicular to the specimen surface (indicated by a red circle at the peripheral of the {011} pole figure). The slip system with the highest Schmid factor, indicated by the red circles in Fig. 2a_5 and a_6, is parallel to the boundaries. As this favorable slip system needs not to cross the boundaries, one would expect all plastic

Table 1
Schmid factor analysis based on the block's Euler angles (φ_1, Φ, φ_2). Because most specimens localize before 2% strain offset, the "critical stress", $\tau_{critical}$, is calculated by multiplying the ultimate tensile strength (UTS) with the block's highest Schmid factor (SF).

Specimen no.	Fig. 2a		Fig. 2b		Fig. 3a		Fig. 3b		Fig. 3c
Block color	Pink	Blue	Red	Blue	Orange	Blue	Red	Blue	Purple
(φ_1, Φ, φ_2)	(11, 23, 309)	(191, 52, 141)	(314, 9, 55)	(142, 57, 234)	(254, 9, 100)	(10, 51, 316)	(26, 6, 335)	(123, 47, 219)	(71, 35, 307)
Highest SF	0.45	0.49	0.44	0.46	0.45	0.47	0.43	0.47	0.48
UTS/MPa	785		873		860		981		871
$\tau_{critical}$/MPa	353	385	384	402	387	404	422	461	418